ANALYSIS OF CHARGE SHAPE INFLUENCE ON BLAST PRESSURE

HRVOJE DRAGANIĆ, SANJA LUKIĆ, IVAN RADIĆ, GORAN GAZIĆ & MARIO JELEČ
Faculty of Civil Engineering and Architecture Osijek, Josip Juraj Strossmayer University of Osijek, Croatia

ABSTRACT

Blast wave intensity depends on several parameters, namely: explosive material type, charge weight, shape and orientation, detonation point position, detonation initiator type (primary explosive type), the position (distance) of the explosive charge in relation to the intended target (standoff distance) and ground surface. Environmental conditions, particularly air temperature, humidity and atmospheric pressure, also influence blast pressures. It is difficult to accurately predict the blast wave action on target structures if all of these parameters are considered. This research concentrates on the influence of the shape of the explosive charge on blast pressure measurements. Spherical and hemispherical charge shapes are considered usual and, as such, accurate and reliable analytical expressions for the blast wave pressure approximation are available. The form and propagation of spherical charge blast waves are considered to have been thoroughly studied and known. In today's urban and guerrilla warfare, speed of action is a crucial factor. Rendering the careful shaping of explosive charges is time consuming and unnecessary, hence the need for investigating different charge shapes, other than spherical. This investigation consisted of field range experimental measurements of the incident (free-field) and reflected pressures caused by detonating differently shaped charges. The shapes considered were: spherical, cylindrical and rectangular. The experiments were numerically validated and verified using ANSYS Autodyn hydrocode software. Numerical simulations utilised a coupled Euler–Lagrange planar solver, using an ideal air environment and PEP500 explosive material. Charge shapes varied, according to the experimental outline, and the measuring points were constant, to allow comparison of the measured data.

Keywords: blast load, charge shape, incident pressure, ANSYS Autodyn.

1 INTRODUCTION

Analytical expressions provide a satisfactory pressure approximation of spherical and hemispherical charges. The propagation of blast waves induced by the detonation of spherical and hemispherical charges is straightforward. The blast wave pressure front expands radially in all directions, as concentric circles from the detonation point. Most research into the blast load on structures is concerned with the blast load produced by spherical charges. Due to thorough research, the blast load from spherical explosive charges is easy to calculate and simulate. Blast load mitigation usually deals with this kind of charge. Today, however, urban and guerrilla warfare mandates speed of action, and so the careful shaping of explosive charges is obsolete and time-consuming. Speed results in arbitrary charge shapes that produce blast pressures and wave propagation, which are different from spherical explosive charges. One of the charge shapes studied in more detail is a cylindrical charge. Recent research emphasises length to base diameter (L/D) as being the main parameter which influences the blast wave shape and pressure distribution. Wu et al. [1] studied the effect of L/D, charge orientation, and scaled distance on blast parameters from the detonation of cylindrical charges, utilising finite element analysis and a small number of experiments. The results indicate that peak reflected pressures and impulses from a vertically-orientated cylinder (with an axis perpendicular to the span of the target) were much larger than those from a spherical charge of equal mass, or a horizontally-orientated cylinder. Sherkar et al. [2], Artero-Guerrero et al. [3] and Langran-Wheeler et al. [4], [5] reported similar findings. Cylindrical

WIT Transactions on The Built Environment, Vol 209, © 2022 WIT Press
www.witpress.com, ISSN 1743-3509 (on-line)
doi:10.2495/HPSU220081

blast parameters are dependent on the detonation initiation point. Studies have shown that pressure can be enhanced by up to three times for centrally-detonated cylinders [6], [7]. Nevertheless, there is a current lack of understanding of the early and mid-stages of blast wave propagation following the detonation of non-spherical charges.

This investigation consisted of field range experimental measurements of incident (free-field) and reflected pressures resulting from the detonation of differently shaped charges. Experiments were numerically simulated using the ANSYS Autodyn® hydrocode software.

2 EXPERIMENT

Experiments were conducted on a military field range, to ensure a safe and secure environment. Military personnel were in charge of explosives handling, charge shaping, placement and detonation. The charges were placed vertically in the tests. Two blast wave parameters, the blast wave incident and reflected pressure, were measured and consequently compared to results obtained by numerical modelling and the empirical expressions derived by Kingery and Bulmash [8].

2.1 Description of explosive

Lead azide detonator capsules initiated the explosive reaction of a PEP500 charge in the field range tests [9]. Lead azide is a primary explosive and it is used as a detonator because it has a very stable shelf life. PEP500 is a secondary plastic explosive with a density of 1.5 g/cm^3 and a detonation velocity of 7,400 m/s. Plastic explosives can be formed in arbitrary shapes with no danger of losing their stability and triggering an accidental explosion. The shape of the PEP500 charge varied in three shapes: spherical, cylindrical and rectangular. Each test consisted of detonating 100 g of plastic explosives and pressure measurements were taken at the same standoff distance. Table 1 lists the charge geometries. Fig. 1 shows the explosive packaging, charge shapes and detonator capsules. Expert personnel of the Croatian army conducted the experimental testing at the field range.

Table 1: Charge shape geometry.

Charge shape	Shape dimensions (mm)							
	Height (*h*)		Width (*w*)		Length (*l*)		Base radius (*r*)	
	M	C	M	C	M	C	M	C
Spherical	/	/	/	/	/	/	27.5	25.0
Cylindrical	100.0	94.3	/	/	/	/	15.0	15.0
Rectangular	30.0	33.0	40.0	40.0	50.0	50.0	/	/

Note: M = field measured dimensions; C = calculated for numerical modelling from mass equation.

2.2 Experimental setup

The field tests consisted of detonating 100 g of PEP500 explosives in different shapes and at a distance of 1.857 m from pressure sensors. Remote detonation utilised an electric discharge from a safe cover, 50 m away. The detonator was placed vertically inside a charge to minimise the influence of positioning on the generated pressures. The cover consisted of the data acquisition system for pressure measurements and the remote detonator. The pressure sensor distance was kept constant throughout each subsequent detonation, to maintain consistency in the measured data. The blast wave incident and reflected pressures were

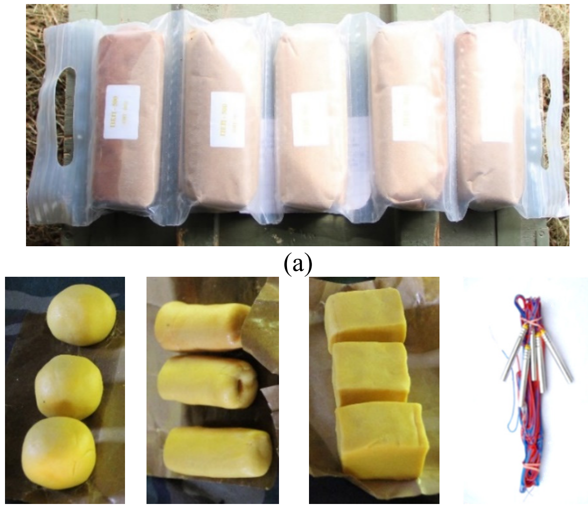

Figure 1: Charge shapes and detonator capsules. (a) Original packaging of plastic explosive PEP500; (b) Spherical; (c) Cylindrical; (d) Rectangular; and (e) Detonator.

measured. The test implemented four quartz free-field ICP® blast pressure pencil probes (PCB 137B23B), to measure incident pressures, and two IEPE® reflected pressure sensors (Dytran IEPE 2300 V6) for measuring reflected pressure. Pencil probes were placed at an equal distance from the centre of the charge in all four directions. Pencil probes were designated as 11126, 11127, 11128 and 11129. Reflected pressure sensors, designated as 5770 and 5771, were placed at an angle of 225°. A wooden stand held the charge at 1.0 m height in all tests. The sensors were placed at the same elevation and oriented to the charge centre. The positions of the probes are shown in Fig. 2. The field range test setup is shown in Fig. 3. Each charge shape was detonated four times, to obtain a larger data set of measured pressures for comparison and analysis. The weight of the explosive is labelled as W, the actual distance from the centre of the explosive to the sensor is R, and the scaled distance is Z. Considering the distance and charge weight, the adopted scaled distance was 4.0 m/kg$^{1/3}$.

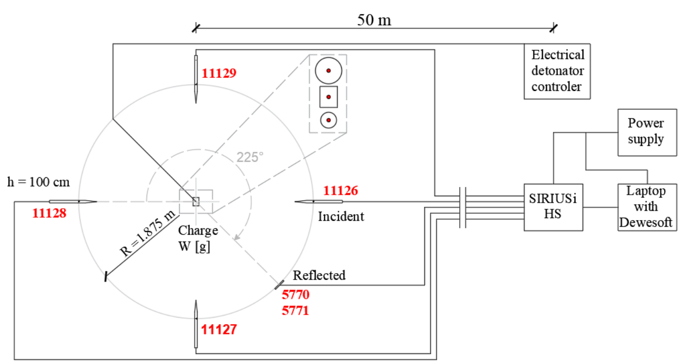

Figure 2: Test setup disposition (location of pressure sensors).

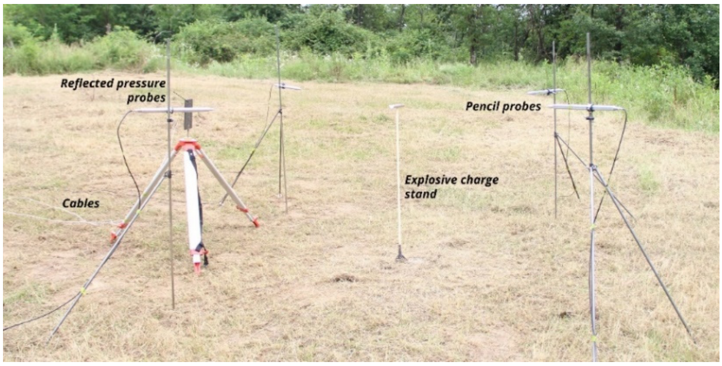

Figure 3: Field range test setup.

Based on previous experience in field blast tests [10], to prevent fireball influence, the charges were not placed too close to the sensors. Fireballs can affect sensors at a distance of 0.835 m ($Z = 1.8$ m/kg$^{1/3}$), so these tests utilised larger distances.

3 NUMERICAL MODELLING

Simulations of experimental tests utilised the ANSYS Autodyn hydrocode software [11]. The numerical models used a planar multi-material Euler Godunov solver [12] and the use of symmetry enabled faster calculation. The model consisted of two parts: air and explosive charge. Air was modelled as an ideal gas while the explosive was PETN1.5, via the Jones–Wilkins–Lee (JWL) equation of state [13]. Air is a gaseous material and solely serves as a transfer medium for the blast waves generated by detonation. The explosive does not have any strength law but it is essential for generating blast waves. Based on the available ANSYS library materials, it was concluded that the PETN1.5 explosive was the one most similar to PEP500.

Table 1 lists the charge shapes and geometrical dimensions used in the field tests. Fig. 1 shows the geometry of the charges. Based on weight, the specific dimensions were calculated and compared to the measured values used in the experiment. The charge weight was considered a constant value throughout all field tests. The calculated geometry parameters for all three charges were approximately the same as the charges detonated, resulting in the minimal influence of charge geometry on the measured blast pressures in the numerical simulations.

A numerical model of the experimental setup is shown in Fig. 4. The symmetry condition allows the modelling of only half of the air environment. The flow out boundary condition is defined on air environment edges to enable free flow of the blast pressures outside the defined air environment, avoiding pressure reflection and amplification. Gauge points 1 (11126), 2 (11127 and 11129) and 4 (11128) measure the incident pressures. As in the experiment, the steel plate is modelled behind gauge point 3 (5770 and 5771), to enable blast pressure reflection and measurement of the reflected pressure. The model setup was similar for all the tests, varying the charge shapes defined in Table 1. A half-circle PETN1.5 fill in an air environment represents a spherical charge, as does the vertically oriented cylindrical charge but with an appropriate base radius. A rectangular PETN1.5 fill with rectangular sides, oriented in the same way as in the field tests, represents a rectangular charge. Length is oriented vertically and height/thickness is oriented laterally. The detonation point is defined in the middle of all simulated charge shapes.

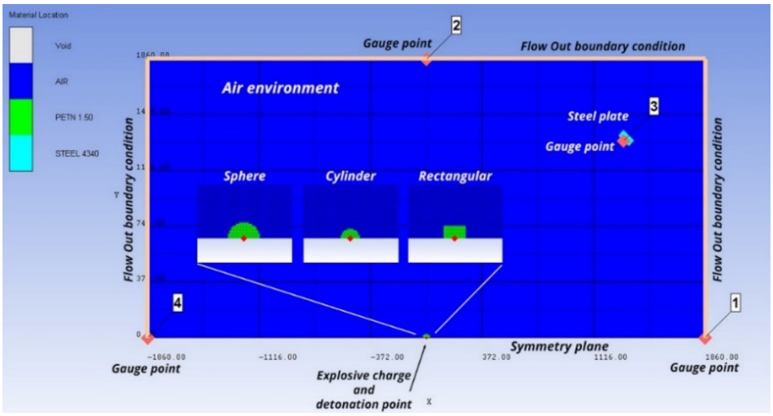

Figure 4: Numerical model of experimental setup.

4 ANALYTICAL CALCULATION

The Kingery and Bulmash (K&B) expressions estimated field pressures for the spherical charge in free-air and as surface burst. The pressure calculation considers both burst types because the reflection of the blast wave from the ground is expected, due to the greater distance of the measuring instruments from the charge (1.857 m) than from the charge to the ground (1.0 m). Incident and reflected pressures were calculated for 100 g of PEP500 explosive (TNT equivalent 1.3). These equations are the basis for predicting pressures and are integrated into various software, such as CONWEP [14]. However, this analysis aims to determine the differences in pressure; do the expressions overestimate or underestimate the measured pressures generated from different charge shapes? The K&B expression for the incident or reflected pressure *Y* calculation is:

$$Y = 10^{(C_0 + C_1 \text{x}\, U + C_2 \text{x}\, U^2 + \cdots + C_N \text{x}\, U^N)} \text{ with } U = K_0 + K_1 \text{x} \log Z, \tag{1}$$

where *Z* is scaled distance, and K_0, K_1, C_0, C_1, $C_2 \ldots C_N$ are Kingery and Bulmash polynomial constants, which can be found in Kingery and Bulmash [8].

5 RESULTS AND DISCUSSION

The experimental results were analysed and compared to the results obtained by K&B equation and numerical simulations in ANSYS Autodyn.

5.1 Experimental results

Four detonations were performed for each charge shape and four incident, and two reflected, pressures were measured during each detonation.

5.1.1 Incident pressure

The diagrams of the distribution of incident pressure versus time are shown in Fig. 5, for all measurement sensors. For the spherical shape, an equal pressure distribution is expected due to the spherical propagation of the blast wave. Differences in the diagrams are possible because of the imperfect sphere shape due to hand moulding. The detonator placed from below results in the pressure diagrams being more uniform over time because the position of the detonator has the same effect on explosive material in all four directions. All measurements have the duration of the positive phase, up to 1.5 ms. A horizontally oriented cylindrical charge is expected to have higher pressures perpendicular to the cylinder but a vertically oriented cylinder will have more uniform pressures in all directions and similar arrival times.

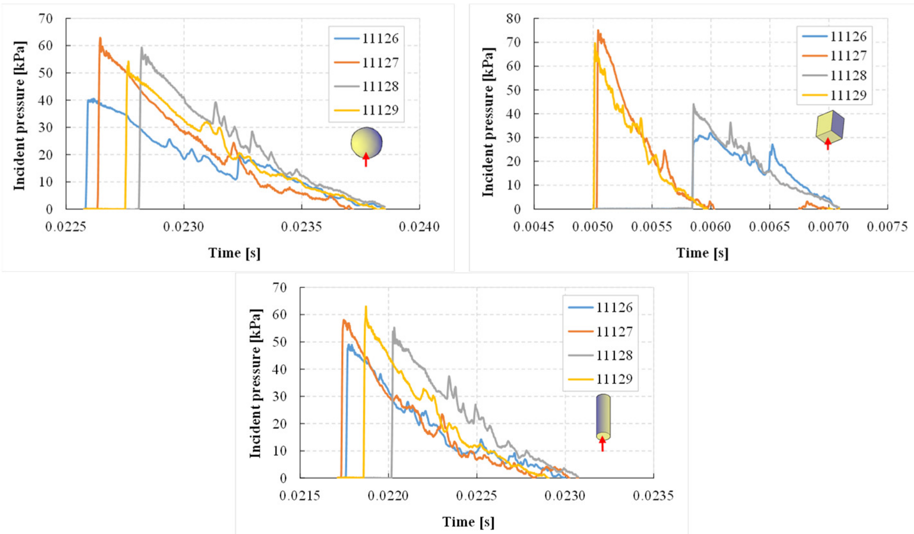

Figure 5: Incident pressure–time diagrams measured for all three charge shapes.

A rectangular charge produced the highest incident pressure of 75.02 kPa. Cylindrical and spherical explosive charges exhibit lower pressure values, 63.06 kPa and 62.89 kPa, respectively. The difference between the maximum measured pressures reached 16% but was within acceptable limits.

Table 2 presents all of the measured pressures. The arithmetic means, the standard deviation, and the coefficient of variation (CoV) were calculated for each sensor. CoV indicates a high reliability of experimental results because deviations are within the allowable limits, i.e. less than 30%.

Table 2: Measured incident pressures (kPa) in all detonations.

	Spherical				Rectangular				Cylindrical			
Detonation	**11126**	**11127**	**11128**	**11129**	**11126**	**11127**	**11128**	**11129**	**11126**	**11127**	**11128**	**11129**
1	48.59	52.63	57.23	51.75	30.22	64.83	28.28	60.64	41.95	53.75	**58.26**	55.32
2	46.79	57.85	45.33	53.89	**27.88**	60.85	34.17	65.23	49.09	58.12	55.27	**63.06**
3	40.60	**62.89**	**59.31**	**54.24**	29.06	68.10	33.46	66.70	51.21	54.27	54.38	55.54
4	48.74	55.07	53.31	53.76	31.98	**75.02**	**43.93**	**69.61**	51.00	57.20	54.66	52.95
x̄	**46.18**	**57.11**	**53.80**	**53.41**	**29.79**	**67.20**	**34.96**	**65.55**	**48.31**	**55.84**	**55.64**	**56.72**
σ	**3.83**	**4.40**	**6.17**	**1.13**	**1.75**	**6.00**	**6.53**	**3.74**	**4.35**	**2.15**	**1.78**	**4.39**
CoV	**8%**	**8%**	**11%**	**2%**	**6%**	**9%**	**19%**	**6%**	**9%**	**4%**	**3%**	**8%**

Note: x̄ = arithmetic mean, σ = standard deviation, CoV = coefficient of variation.

Pressure–time diagrams measured on sensor 11128 for all charge shapes are shown in Fig. 6(a). The rectangular charge gives the lowest pressures on this sensor, while the minimum differences are between the sphere and cylinder. Experimental measurements did not contain the arrival time and, because of that, when comparing results, the maximum pressures were set at the same instance.

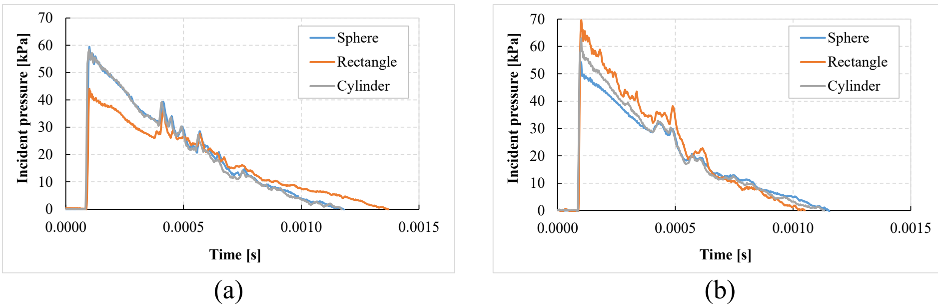

Figure 6: Measured incident pressure–time diagrams. (a) Sensor 11128; and (b) Sensor 11129.

The diagrams in Fig. 6(b) show pressures for the lateral sensor 11129, perpendicular to the direction of charge. The records show a uniform appearance of the pressure diagram for all three charge shapes. The difference lies in the peak pressure values; the rectangular shape shows a slightly pronounced pressure peak, while the sphere shows the lowest peak pressure.

5.1.2 Reflected pressure

Table 3 presents the measured reflected pressures. The most uniform measurements are for the sphere (coefficient of variation (CoV) 7%), then the rectangle (from 9% to 13%), and the cylinder (from 5% to 20%). The CoV of 20% for sensor 5771 indicates significant differences in measurements but is still within acceptable limits.

Table 3: Measured reflected pressures (kPa).

	Spherical		Rectangular		Cylindrical	
	5770	**5771**	**5770**	**5771**	**5770**	**5771**
Bottom	188.84	258.47	246.62	308.46	188.31	230.44
	176.11	277.59	189.76	277.17	205.06	314.72
	192.86	297.82	244.35	311.17	193.48	200.19
	210.44	298.66	208.16	258.39	182.11	282.38
$\bar{x}$	**192.06**	**283.13**	**222.22**	**288.80**	**192.24**	**256.93**
σ	**14.18**	**19.11**	**27.91**	**25.47**	**9.73**	**51.34**
CoV	**7%**	**7%**	**13%**	**9%**	**5%**	**20%**

Note: $\bar{x}$ = arithmetic mean, σ = standard deviation, CoV = coefficient of variation.

The diagram in Fig. 7 shows the reflected pressures measured on sensor 5770 during the detonation of all three shapes. The diagrams are uniform, which indicates the accuracy of the measurements. For the detonator placed vertically, measurements show the highest reflected pressures for the rectangle.

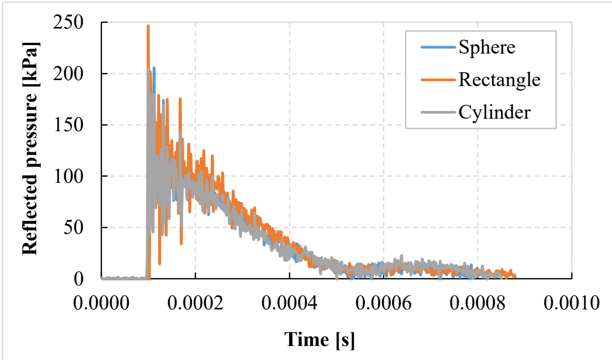

Figure 7: Reflected pressure–time diagrams measured by 5770.

5.2 Numerical results

The sphere was modelled as an axisymmetric (1D) model with a mesh size of 1 mm for air elements and is used for K&B calculated pressures verification. The base model for simulating experimental tests was a 2D planar model with a mesh size of 2.5 mm.

5.2.1 Incident pressure

Incident pressures were measured with a gauge 4 sensor (11128) for all charge shapes and are shown in Fig. 8(a). Comparing the diagrams of the incident pressures obtained numerically, the difference in arrival time of the blast wave to the sensor is also visible. There is also a difference in the measured pressure values. The smallest value of measured pressure is for the cylinder. The difference in value is almost 30 kPa, in comparison with the spherical charge.

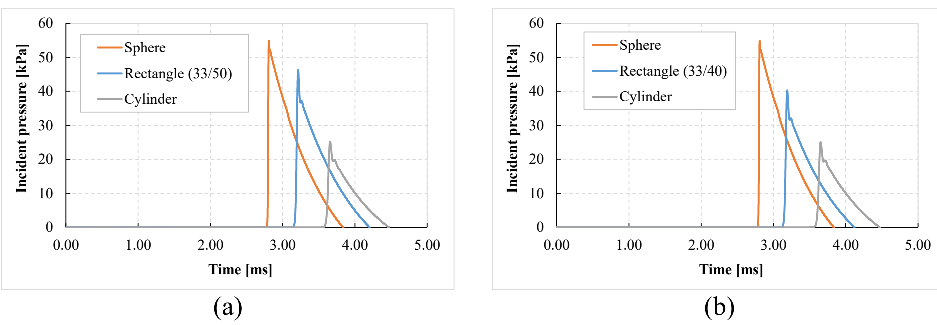

Figure 8: Numerically simulated incident pressure–time diagrams. (a) Gauge 4 (11128); and (b) Gauge 2 (11127 and 11129).

The pressures were measured at the lateral gauge point (2), perpendicular to the charge axis. Data correspond to the results of experimental measurements on sensors 11127 and 11129. The diagrams are uniform for all three shapes (Fig. 8(b)) but differ in their maximum value. The pressures measured for the sphere and cylinder are the same as for gauge 4, which was expected because of the circular charge shape and uniform blast wave propagation.

5.2.2 Reflected pressure

The reflected pressure was measured at point 3, shown in Fig. 4. The reflected pressure diagrams follow the trend of the incident pressure diagrams but are of greater intensity (Fig. 9). A vertically placed detonator results in the lowest reflected pressures for the cylinder and the highest for the spherical charge detonation.

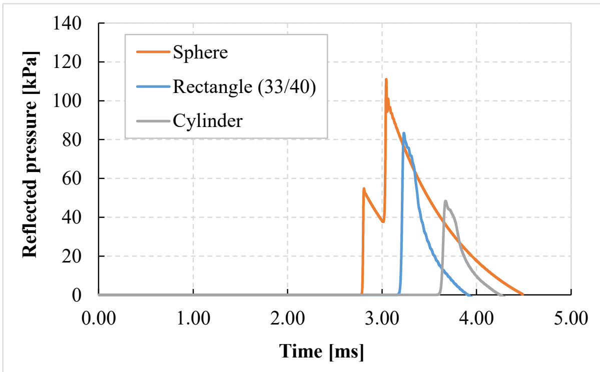

Figure 9: Reflected pressure–time diagrams measured on the gauge 3 (5770 and 5771).

5.3 Kingery Bulmash expression

Eqn (1) provides pressure values for charges placed in the air (A) (sphere) and on the surface (S) (hemisphere). Table 4 lists the K&B values. Incorporating the shape as a parameter in K&B expressions is not applicable. The pressures obtained for the sphere served in the comparison of all detonation scenarios.

Table 4: Values obtained via Kingery and Bulmash expressions.

Parameters			**Kingery and Bulmash**				
W (kg)	R (m)	TNT equivalent	Position	Incident (kPa)	Reflected (kPa)	t_a (ms)	t_d (ms)
0.100	1.857	1.3	Air (A)	54.90	133.50	2.8	1.50
0.100	1.857	1.3	Surface (S)	76.90	199.00	2.5	1.65

Note: t_a = arrival time, t_d = positive phase duration.

5.4 Result comparison

The arithmetic mean of the experimentally determined (incident and reflected) pressures for different charge shapes and the pressure values determined by the Kingery and Bulmash expression, are shown in Fig. 10.

A comparison of experimental and K&B results shows that K&B overestimate the pressures (Fig. 10(a)). Significantly higher pressures were recorded by the lateral sensors (11127 and 11129) for all charge shapes, especially for a rectangular charge. The measured results coincide with K&B results when the charge is placed in the air, which is to be expected. According to Fig. 10(b), it can be seen that all of the reflected pressures measured experimentally were closer to the value for the surface burst obtained via K&B.

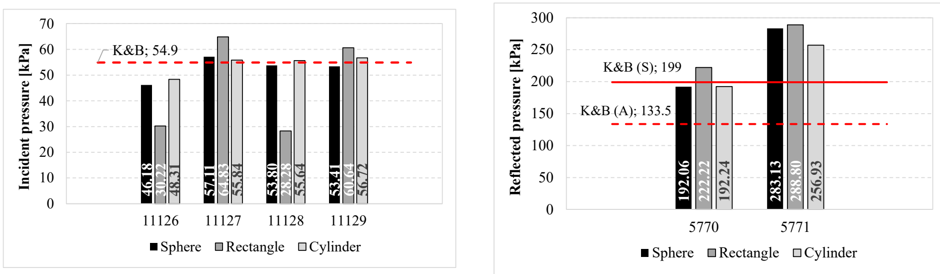

(a) (b)

Figure 10: Arithmetic mean of measured pressures. (a) Incident pressures; and (b) Reflected pressures.

A sphere modelled in 1D axisymmetry gives better matches with K&B than modelling in 2D because of a finer mesh (1 mm) which provides more accurate results. For the sphere, the incident pressures obtained were the same as those found through the K&B expression, while the rectangular and cylindrical charges produced lower pressures (Fig. 11). The comparison indicates the difference in pressures for different charge shapes.

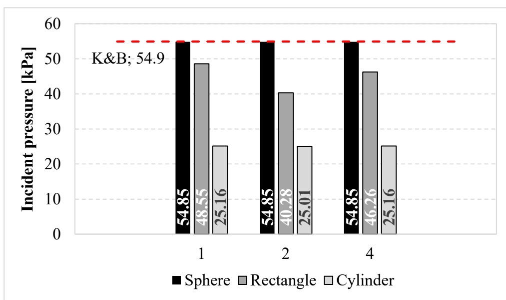

Figure 11: Numerically obtained incident pressures.

Comparing the numerically obtained reflected pressures with K&B, they are lower than the pressures obtained via the K&B expression for a charge in free-air. In the experimental results, the measured pressures were higher than those obtained for K&B for a surface charge.

A comparison of the numerically determined pressures with the arithmetic mean of the experimentally determined ones shows a good agreement of the results, considering the spherical charge. For the rectangular shape, experimentally similar pressures were measured with sensors 11126 and 11128, which are lower than the numerically determined pressures at these locations. With sensors 11127 and 11129, pressures twice as high as those measured with sensors 11126 and 11128 were measured, and these pressures were higher than the numerically determined pressures. It is believed that the differences are due to the fact that the numerical model was created in a 2D simulation and the third dimension of the charge shape, which also affects the measured pressure, was neglected. This problem also occurred with the cylinder because the influence of the height of the cylinder on the measured pressure is neglected in the numerical simulation. After detonation of the cylinder, uniform pressures were measured at all sensors, which is to be expected because the cylinder is vertical, but the experimental pressure measurements were more than twice the numerically determined pressures; the results are shown in Fig. 12.

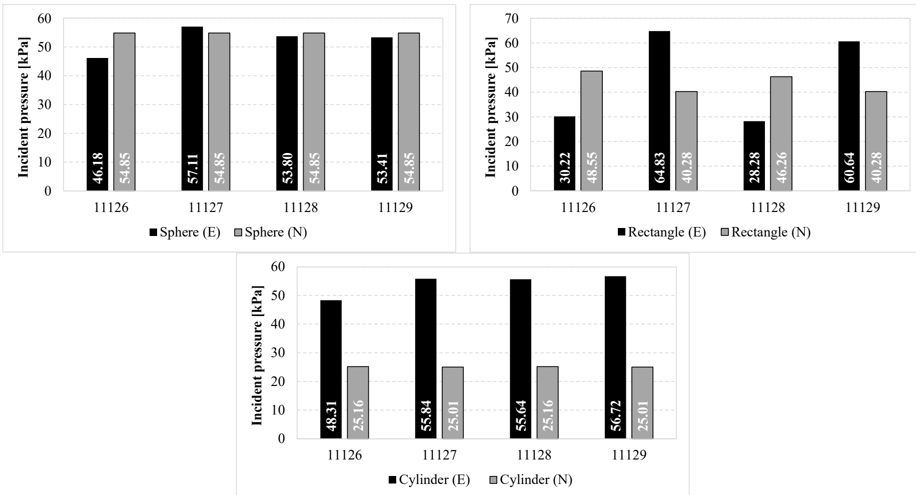

Figure 12: Comparison of experimentally measured and numerically determined pressures.

6 CONCLUSION

The Kingery and Bulmash equation predicts the pressures well for the spherical charge. The deviations from the experiments and the expression are minimal. Numerical simulations can also give identical pressures using a simple 1D model with a mesh size of 1 mm. When rectangular and cylindrical explosive charges are considered, the comparison yields significant discrepancies. For vertically oriented explosives, K&B estimates pressures well for these two shapes. It is recommended that the influence of shape and orientation be further investigated by increasing the weight of the charge and varying the standoff distance. In numerical simulations, K&B overestimates the pressures for the rectangle and cylinder. The numerically determined reflected pressures are much lower than the pressures measured experimentally and calculated by K&B. Due to the limited capacity of computer hardware, only 1D and 2D models are considered in this paper. This should be extended to 3D simulations to include all three charge dimensions, since 2D simulations are spatially limited.

ACKNOWLEDGEMENTS

This paper was supported, in part, by the Croatian Science Foundation (HRZZ) under the project (UIP-2017-05-7041) “Blast Load Capacity of Highway Bridge Columns”, and support for this research is gratefully acknowledged. The authors would also like to thank the Croatian Army for providing all the necessary support in conducting blast measurements in the form of recommendations, access to the training ground, and securing the explosive material.

REFERENCES

[1] Wu, C., Fattori, G., Whittaker, A. & Oehlers, D.J., Investigation of air-blast effects from spherical-and cylindrical-shaped charges. *International Journal of Protective Structures*, **1**, pp. 345–362, 2010.

[2] Sherkar, P., Shin, J., Whittaker, A. & Aref, A., Influence of charge shape and point of detonation on blast-resistant design. *Journal of Structural Engineering*, **142**, 04015109, 2016.
[3] Artero-Guerrero, J., Pernas-Sánchez, J. & Teixeira-Dias, F., Blast wave dynamics: The influence of the shape of the explosive. *Journal of Hazardous Materials*, **331**, pp. 189–199, 2017
[4] Langran-Wheeler, C., Tyas, A., Rigby, S., Stephens, C., Clarke, S. & Warren, J., Characterisation of reflected blast loads in the very-near field from non-spherical explosive charges. *Proceedings of the 17th International Symposium for the Interaction of Munitions with Structures (ISIEMS17)*, 2017.
[5] Langran-Wheeler, C., Tyas, A., Rigby, S., Stephens, C., Clarke, S. & Walker, R., Reflected blast loads from long cylinders in the near-field. *Proceedings of the 18th International Symposium for the Interaction of Munitions with Structures (ISIEMS18)*, Panama City, FL, 2019.
[6] Hu, Y., Chen, L., Fang, Q. & Xiang, H., Blast loading model of the RC column under close-in explosion induced by the double-end-initiation explosive cylinder. *Engineering Structures*, **175**, pp. 304–321, 2018.
[7] Xiao, W., Andrae, M. & Gebbeken, N., Influence of charge shape and point of detonation of high explosive cylinders detonated on ground surface on blast-resistant design. *International Journal of Mechanical Sciences*, **181**, 105697, 2020.
[8] Kingery, C.N. & Bulmash, G., Airblast parameters from TNT spherical air burst and hemispherical surface burst. US Army Armament and Development Center, Ballistic Research Laboratory, 1984.
[9] Ngo, T., Mendis, P., Gupta, A. & Ramsay, J., Blast loading and blast effects on structures: An overview. *Electronic Journal of Structural Engineering*, **7**, pp. 76–91, 2007.
[10] Lukić, S., Draganić, H., Gazić, G. & Radić, I., Statistical analysis of blast wave decay coefficient and maximum pressure based on experimental results. *WIT Transaction on The Built Environment*, vol. 198, WIT Press: Southampton and Boston, pp. 65–78, 2020.
[11] ANSYS I, ANSYS Autodyn user manual (Release 15.0). ANSYS, 2013.
[12] Kohnke, P., ANSYS Theory Manual, Release 12.0. ANSYS Inc., 2009.
[13] Draganić, H. & Varevac, D., Numerical simulation of effect of explosive action on overpasses. *Građevinar*, **69**, pp. 437–451, 2017.
[14] Hyde, D.W., Microcomputer programs CONWEP and FUNPRO, Applications of TM 5-855-1, "Fundamentals of Protective Design for Conventional Weapons" (User's Guide). Army Engineer Waterways Experiment Station, Vicksburg MS, Structures Laboratory, 1988.